Time-of-Flight Characterization of Electrospray Thrusters Using Porous Emitters with High Emission Currents

Chengyu Ma*, Thomas Bull† and Charles N. Ryan‡
University of Southampton, Southampton, Hampshire, the United Kingdom, SO17 1BJ

An electrospray thruster designed for nanosatellites is introduced in this paper. The thruster has a compact size featuring a passive propellant transport method through the use of porous materials. Porous electrospray emitters with 1, 25 and 100 emission tips were fabricated using conventional machining techniques. The geometrical features of the emission tips were analysed based on the measurement using a high-precision laser profilometer. Thruster prototypes fitted with different emitters were tested in a bipolar operation mode. The emission currents and voltage characteristics were studied, which demonstrated a wide range of operational voltage with relatively high emission currents. The maximum overall emission currents were +3.22 mA and -4.72 mA achieved at ±3500 V, and the maximum emission current per emission tip was +93.2 μA and -100.8 μA at +3067 and -3118 V, respectively. Time-of-flight systems were utilised to characterise the mass and velocity distribution of the charged particles in the thruster plume. The results suggested that the electrospray emission were highly ionic with mostly monomer and dimer ions present. The thruster performance was conservatively estimated, with the thrust ranging from approximately 1 μN to 204 μN, and the specific impulse ranging from 3000 s to approximately 6000 s.

Nomenclature

d_{EE}	=	distance between the emitter and the extractor, mm
f_l	=	the fraction of ToF collected current representing light species
$I(t)$	=	electric current received on the time-of-flight collector varying over time, A(s)
Isp	=	specific impulse, s
L	=	flight distance between time-of-flight gate and collector, m
m	=	mass of the charged particle, kg
$\dot{m}$	=	mass flow rate, kg/s
P_{in}	=	input power, W

*Ph.D. Candidate, Aeronautics, Astronautics and Computational Engineering, Faculty of Engineering and Physical Sciences, SO17 1BJ
†Post Doctoral Researcher, Mechatronics Research Group, Faculty of Engineering and Physical Sciences, SO17 1BJ
‡Lecturer in Astronautics, Aeronautics, Astronautics and Computational Engineering, Faculty of Engineering and Physical Sciences, SO17 1BJ

P_{jet} = jet power, W

q = electric charge of the particle, C

r_x, r_y = the principle curvature radii in perpendicular axes of a point on the cone surface, μm

T = thrust, N

V_{ac} = acceleration voltage, V

η = efficiency

θ_x, θ_y = two perpendicular angles of the particle flying vector relative to the overall thrust vector, degrees

ω = specific charge ratio of heavier species to light species

Subscripts

ang = angular

i = ionization

nk = non-kinetic

poly = polydispersive

t = time of flight

th = theoretical

tr = transmission

I. Introduction

With the development of miniaturized electronics, nanosatellites have demonstrated their capabilities to complete satellite missions at a fraction of the cost of a conventional satellite. In the past decade, CubeSats have developed from an educational tool to more sophisticated commercial and scientific applications, such as formation flying missions [1], low-earth-orbit constellations [2] and deep space explorations [3]. Although not prevalent currently, being equipped with an onboard propulsion system CubeSats can further improve their mission competence. For example, in low earth orbit, a micro-propulsion system can compensate for atmospheric drag on a CubeSat and extend its orbiting lifetime. For a remote sensing or imaging nanosatellite, the pointing accuracy can be improved by using thrusters for precise attitude control. Missions requiring high-velocity changes, such as orbit changing, can be enabled using a propulsion system with high specific impulse. However, the development of micro-propulsion technologies is challenging due to the size and power supply constraints on a nanosatellite. Among all the micro-propulsion systems currently being developed [4, 5], including cold-gas, monopropellant and electric micro-propulsion systems, electrospray propulsion [6] and field emission electric propulsion [7] are particularly promising due to their high specific impulse and high power efficiency at low power. In general, electrospray thrusters are capable of achieving high specific impulse over 1000 s while maintaining a relatively high efficiency around 40% at power lower than 20 W [8]. The efficiency of electrospray

thrusters is usually higher than most other electric propulsion systems, whose power efficiency noticeably decreases when their powers are scaled down to tens of Watts, including miniature Hall effect thrusters [9] and gridded ion thrusters [10]. The high specific impulse and efficiency of electrospray thruster make them one of the few high-performance electric propulsion systems suitable for nanosatellites [11].

In an electrospray thruster, an electric field is applied to the liquid propellant, and the equilibrium condition between the liquid surface tension and the surface electrical stress results in the formation of a conically shaped liquid meniscus, termed a Taylor cone, from whose tip usually a jet is formed and breaks into droplets, generating thrust. If the liquid propellant has a high electrical conductivity and surface tension along with a low flow rate, the surface electrical stress on the Taylor cone tip will be strong enough to break the ionic bond between cations and anions of the molecules on the liquid surface. This results in the extraction and acceleration of solely ions with no droplets present, yielding a higher specific impulse, typically over 1000 s [12, 13]. Some room temperature ionic liquids with such properties have proven suitable as electrospray propellants that can achieve purely ionic emission [14]. Although electrospray thrusters in purely ionic emission regime can offer a high specific impulse, the thrust generated from one Taylor cone is generally found to be around 0.1 μN [15–17], which although could be suitable for precise attitude control, the thrust value is generally too low for a wide range of practical applications.

In order to increase the electrospray thrust while keeping high specific impulse, several computer-numerical-controlled (CNC) machined porous glass emitters are investigated in this paper. These CNC machined emitters have relatively large tip sizes, where more emission sites are expected to occur. The emitter manufacturing quality was measured using a high-precision laser profiling system and the geometrical data was analysed. The emitters were tested in a vacuum chamber and their current-voltage curves were collected. The compositions and velocity distributions of the plume particles were characterized using time-of-flight (ToF) systems. The testing results were used to calculate the specific impulse and thrust of the measured particles. The propulsive performance of the thruster can be estimated based on the ToF results.

II. Porous emitter electrospray thruster design and manufacturing

The electrospray thrusters introduced in this paper are termed porous-emitter electrospray thruster, PET-100-MK1 thruster. The PET-100-MK1 thruster configuration is illustrated in Figure 1. The thruster consists of an extractor electrode, a porous emitter, a porous propellant reservoir, an optional porous nickel distal electrode and a perforated aluminium electrode. Apart from the extractor mounted outside the thruster enclosure, all the other thruster components were stacked inside the thruster enclosures, which were additively manufactured via 3D printing of high-detail resin material.

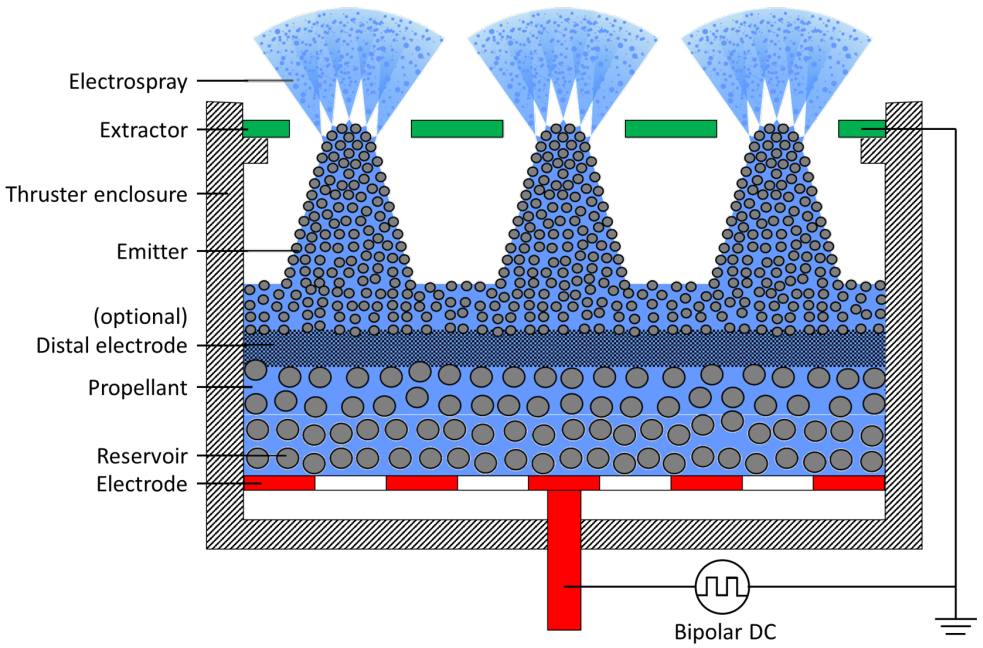

Fig. 1 Illustration of the working principle of the developed porous emitter electrospray thruster.

A. Electrospray thruster design

A manufactured PET-100-MK1 thruster is illustrated in Figure 2(a). Including the emission tips, the overall size of the emitter substrates was $30 \times 30 \times 7$ mm. The extractor grid of the PET-100-MK1 thruster was water-jet cut from a 0.25 mm thick stainless steel sheet with 100 apertures of 1.5 mm diameter. The propellant reservoir was a round porous glass substrate with a size of $\Phi 30 \times 3$ mm. The distal electrode was a 2 mm thick porous nickel substrate, placed between the emitter and the reservoir. Compared to most other ionic liquids, EMI-BF_4 has a relatively high conductivity of approximately 1.36 S/m at room temperature, but this is still significantly lower than that of Nickel, which is 1.43×10^7 S/m. As a result, the propellant experiences potential drops at the porous borosilicate emitter and propellant reservoir parts, while the ionic liquid at the distal electrode part has a nearly consistent electric potential. During electrospray emission, the counter-ions from the emission would accumulate at the surrounding solid surface and flow toward the upstream via diffusion and the electrostatic force. When the counter-ions reach the porous nickel distal electrode where the electrostatic field is weak enough to be neglected, the transport of species would be slow down via solely dominated by the diffusion. The large internal surface area in the porous nickel distal electrode helps to mitigate the detrimental electrochemical reactions that normally occur at emitter tips [18]. Notably, the effectiveness of such electrochemistry mitigation will be compromised at higher emission current, where the generation rate of the counter-ions becomes too high for the diffusion rate to match.

The ionic liquid propellant studied and tested in PET thrusters was 1-Ethyl-3-methylimidazolium tetrafluroborate (EMI-BF_4), which has relatively high surface tension of 4.52×10^{-3} mN/m and high electrical conductivity of 1.36 S/m.

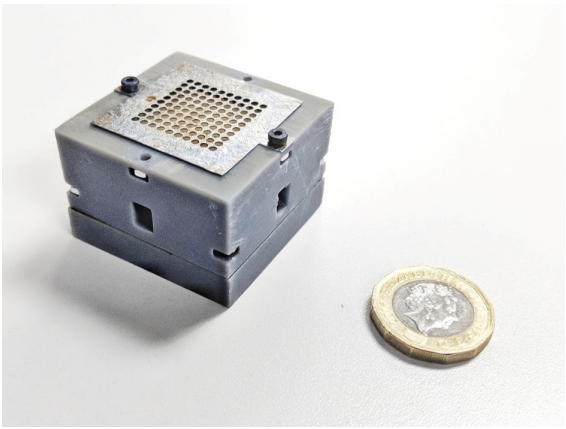

(a) The PET-100-MK1 thruster.

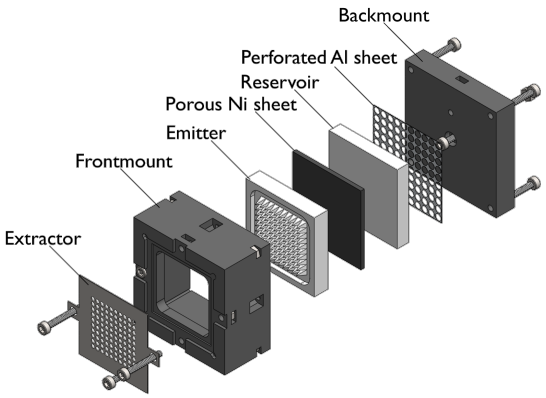

(b) Exploded view of the PET-100-MK1 thruster.

Fig. 2 Design of a PET-100-MK1 thruster.

It has been widely used as an electrospray propellant and demonstrated good performance in terms of specific impulse [11]. In addition, EMI-BF_4 has negligible vapor pressure, making it possible to adapt the design of a non-pressurized propellant storage reservoir.

The propellant transport design is based on a passive method utilizing capillary action [19]. The propellant reservoir was made from a P0 grade porous material. The nominal value of the maximum pore size in a P0 porous glass ranges from 160 to 250 μm, which was larger than the nominal pore size of the emitters. Depending on the thruster configuration, the reservoir was either in contact with the emitter or with the distal electrode. The Laplace pressure between the liquid interfaces on the emitter side and on the reservoir side would spontaneously be balanced; therefore, during electrospray process, as the emitted particles would create an additional Laplace pressure difference, new propellant would be passively transported from the reservoir to the emitter tips.

With the passive propellant transport method and the non-pressurized propellant reservoir, the PET-100-MK1 thruster prototype had a compact design that can easily fit in a nanosatellite. Due to its modular shape, multiple PET-100-MK1 thrusters can be paralleled for higher multiplexed thrust output for microsatellite applications. In addition, the size of the propellant reservoir can be changed depending on the velocity change requirements of different missions.

B. Porous emitters tested

The porous emitter in the PET-100-MK1 electrospray thruster has one or an array of protruding structures, termed emission tips, on whose tip the emission occurs. Compared to the other two major emitter types, capillary emitters [20] and externally-fed emitters [21], porous emitters have been demonstrated capable of housing multiple emission sites on the apex surface of one emitter [19], as illustrated in Figure 1. As a result, porous emitters have the potential of generating a higher thrust in a highly ionic emission regime, for example, a thrust of 150 μN was achieved using 9 prism emitters [22].

(a) A single tip emitter with 20 degrees side surface angle.

(b) A P4 grade emitter with 25 two-millimetre tall tips.

(c) A P5 grade emitter with 100 two-millimetre tall tips.

Fig. 3 The iterations of CNC machined emitters for PET-100.

Other studies have investigated using conductive porous materials as the emitter material, such as porous nickel [23] and porous tungsten [24]. In comparison, multiple studies showed that emitters made of dielectric materials are less affected by the electrochemical reactions that usually occur during electrospray [16]. In order to extend the thruster lifetime, the emitters studied in this paper were made from porous borosilicate glass.

To produce electrospray emitter tip arrays, various manufacturing methods have been utilized. For example, reactive ion etching has been used to fabricate capillary emitters and externally-fed emitters [12, 25], and electrochemical etching has been used to fabricate porous metal emitters [26]. Investigated methods to manufacture porous glass emitters include CNC machining [27], the use of a mold to sinter particulate materials [28] and laser ablation [16]. CNC machining has been used to produce arrays of well formed prism-shaped porous glass emitters [27], which demonstrated a relative high thrust per unit length from the prism edges. Compared to other manufacturing techniques utilized for porous glass emitters, CNC machining is a relatively low-cost and fast process, and consequently, it was used to manufacture emitters for the PET-100-MK1 thruster design. All the emitters discussed in this paper were CNC machined from a 7.5±0.2 mm thick borosilicate porous glass disc with a diameter of 120 mm sourced from VWR International LLC. The porous glass disks which the emitters were manufactured from were P4 and P5 grades, the nominal values of whose maximum pore sizes are from 10 to 16 μm and from 1.0 to 1.6 μm, respectively.

To demonstrate the emission performance of a single porous glass emitter tip, several P4 grade single-tip emitters were studied first. These emission tips had the same height of 5 mm but with different side surface angles of 10, 20 and 30 degrees. In an attempt to increase the overall thrust output, electrospray sources were multiplexed into an array. Therefore, several iterations of emitters with an array of emission tips were then manufactured and tested, including 25 tip emitters and 100 tip emitters, as shown in Figure 3. The pitch distance of the 5×5 emission tip array was 4 mm, and 2 mm for the 10×10 array. In order to machine the tip arrays on the substrate, a one-millimetre diameter ball nose end mill was swept layer-by-layer along two perpendicular horizontal axes. After the machining, the emitters were cleaned with deionised water using an ultrasonic cleaner and then rinsed using acetone to remove the machining coolant and other impurities contained inside the porous materials. The manufacturing results are shown in Figure 3.

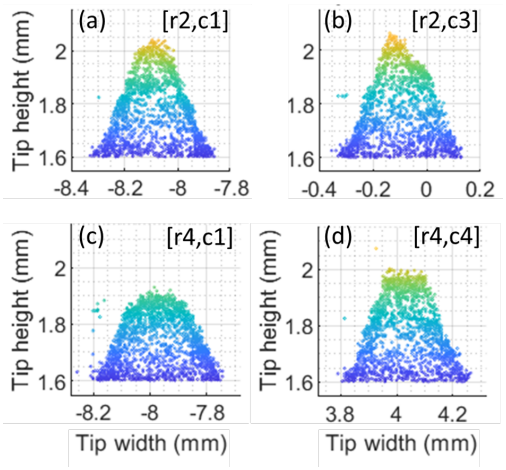

(a) Side view of the four typical emission tips, and r, c values indicate the row and column numbers of the emission tip in the array.

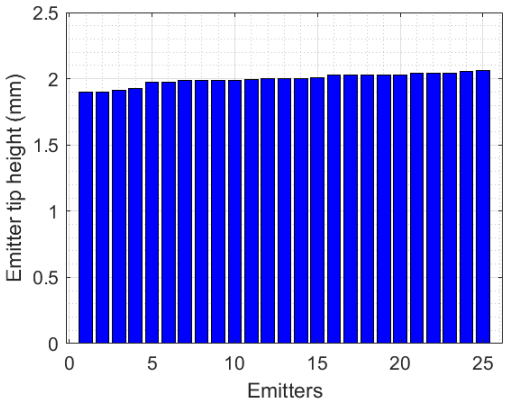

(b) Emission tip height of 25 emission tips.

Fig. 4 Scanning results of a 25-tip emitter.

III. Emitter scanning results

In order to verify the quality of the machined emitters, the emitters were scanned using an XYRIS 2000 WL (3300P) 3-axis confocal laser profiling system, with a minimum positional resolution of 100 nm. A P4 grade 25-tip emitter and a P5 grade 100-tip emitters were scanned, and their scanned data was processed to rebuild the emitter geometry.

A. Scanning of a P4 grade 25-tip emitter

The 25-tip emitter was scanned with a measurement step of 8 μm. The scanned data was then processed using MATLAB, and the side views of the 25 tips are shown in Figure 4(a). Based on the scanning data, the emission tip height and radius distribution of the 25-tip emitter is summarized in Figure 4. The mean height of the emission tips is approximately 1.997 mm with a standard deviation of 45.6 μm. Depending on the geometry of the emitter tip, these 25 emitters can be categorized into four types, which have different potential influences on its experimental performance. Most of the manufactured emitter tips have reasonably good symmetricity along its central axis, among which some tips are relatively sharp, and some are relatively blunt. Given that all the other configurations are the same, sharp tips and blunt tips would have different electric field strength, hence different onset voltages. A small proportion of manufactured tips have asymmetric geometries, with the tip leaning over one side. Although these inclined tips can be relatively sharp, the electric field near the tip would also be asymmetric, potentially resulting in a slanted plume profile. There are also a few outlier emitter tips that are broken during the CNC machining process. These fractured tips could result in a much higher onset voltage, and their near-flat surface would cause more variations of the plume profile.

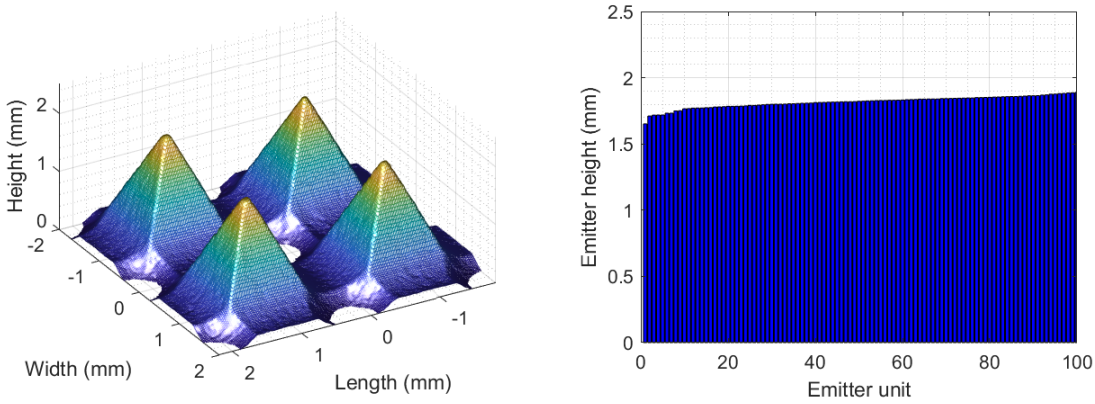

(a) Zoomed-in four typical emission tips.

(b) Emitter height distribution of 100 emission tips.

Fig. 5 Height distribution of the P5 grade 100 emitter tips array.

B. Scanning of a P5 grade 100-tip emitter

For the 100-tip emitter, the overall scanning of the emitter tip array was completed with a measurement step of 20 μm, followed by detailed scanning of single emitter tips with a finer resolution: 5 μm for P5 grade emitters and 8 μm for P4 grade emitters. The scanning result of a typical adjacent four tips in the P5 grade 100 tip emitter array is shown in Figure 5(a). The height data of all emitter tips is shown in Figure 5(b). Most emitter tips are sharp with a relatively good uniformity, but a few emitters have clipped tips, which have larger equivalent tip curvature radii than other sharp tips. The mean height of the P5 grade emitter array tips is 1.816 mm with a standard deviation of 44 μm, and the mean tip radii is 42.3 μm and a standard deviation of 18.5 μm. Excluding the outlier of the clipped tip with a height of 1.652 mm, the mean tip height is 1.818 mm with a standard deviation of 40.8 μm and the mean tip radii is 41.5 μm with a standard deviation of 17.4 μm. Compared to P5 grade emitter tips, the P4 grade material has larger pores and thus weaker structural integrity, resulting in blunter emitter tips. The overall scanning shows that the P4 grade emitter tip array has a mean height of 1.996 mm with a standard deviation of 86 μm, and the mean value of apex radii is 102.5 μm with a standard deviation of 37.6 μm. The height and apex radii standard deviations values are relatively large, and could result in adverse effects on the electrospray emission performance.

Overall the confocal laser profiling results showed that reasonably sharp emitter arrays can be manufactured using CNC machining, although the average radii of these emitter tips are large compared to some porous emitters manufactured using other methods. For example, emitters manufactured using laser ablation can achieve a mean tip radii of approximately 15 μm, and these emitter tips were paired with an extractor that has an aperture size of 0.3 mm in diameter. The extractor was situated directly above the emitter tips, resulting in an onset voltage around 870 V [16]. In comparison, the average tip radii of the CNC machined emitters in this paper are approximately 3 to 5 times as large, and these emitters were paired with an extractor whose aperture diameter is 5 times large. As a result, the onset voltage

of this porous emitter electrospray thruster is expected to scale up to several thousand volts, a voltage achievable from a developed power processing unit. Therefore this level of emitter tip sharpness was deemed satisfactory for the testing of the electrospray thruster.

IV. Experimental system set up

The PET-1 thruster and PET-100-MK1 thruster were tested in the David Fearn Electric Propulsion Laboratory. The vacuum chamber is 4 m long and 2 m in diameter, fitted with one roughing pump, two turbo-pumps with a pumping rate of 2100 L/s of nitrogen each, and two cryopanels that have a pumping rate of 1.5×10^4 L/s of xenon each. The chamber pressure during thruster operation was around 9.8×10^{-7} mbar.

A. Electrical setup and current measurement system

The testing set up is illustrated in Figure 6. The emitter voltage was supplied by two HCP 35-3500 high voltage power supplies from FuG Electronik GmbH, which can output a high voltage from -3500 V to +3500 V with a maximum current of 10 mA. The thruster was tested in bipolar mode where the polarity of the emitter was periodically altered, mitigating detrimental electrochemical effects on the emitter. A high voltage switching unit was used to mechanically switch the output voltage between these two inputs, following the frequency of a square wave from a function generator.

In order to acquire the emitter and extractor current data, a resistor was connected outside the vacuum chamber in series from the power supply to the emitter. Similarly another resistor was connected between the extractor and the ground. In order to reduce the voltage losses from the measuring resistors, 100 kΩ resistors were selected for the current measurement of PET-1 thrusters whose current went up to tens of microamperes, while 10 kΩ resistors were selected for PET-100 thrusters whose maximum current went up to a few milliamperes. The measuring metal film resistors were sourced from TE connectivity, with their resistance measured at room temperature being within ±1% variation from the nominal values. During electrospray emission, the electric potentials before and after the measuring resistors were proportionally reduced to low potentials (<5 V relative to the ground) using high-resistance (>100 MΩ) potential dividers. The low-voltage potential drops were then amplified using an AMP04 amplifier and recorded using a Teledyne LeCroy WaveSurfer 3034Z oscilloscope.

Inside the vacuum chamber, the thruster was mounted on a rotational platform, which can be remotely controlled to change the direction of the thruster, allowing measurements by different probes, including a full emission current collector and a time-of-flight system. The full emission current collector is a 150 × 150 mm aluminium plate fitted with two grids in its front: one outer grid that is grounded, and one negatively charged grid to suppress secondary electron emission.

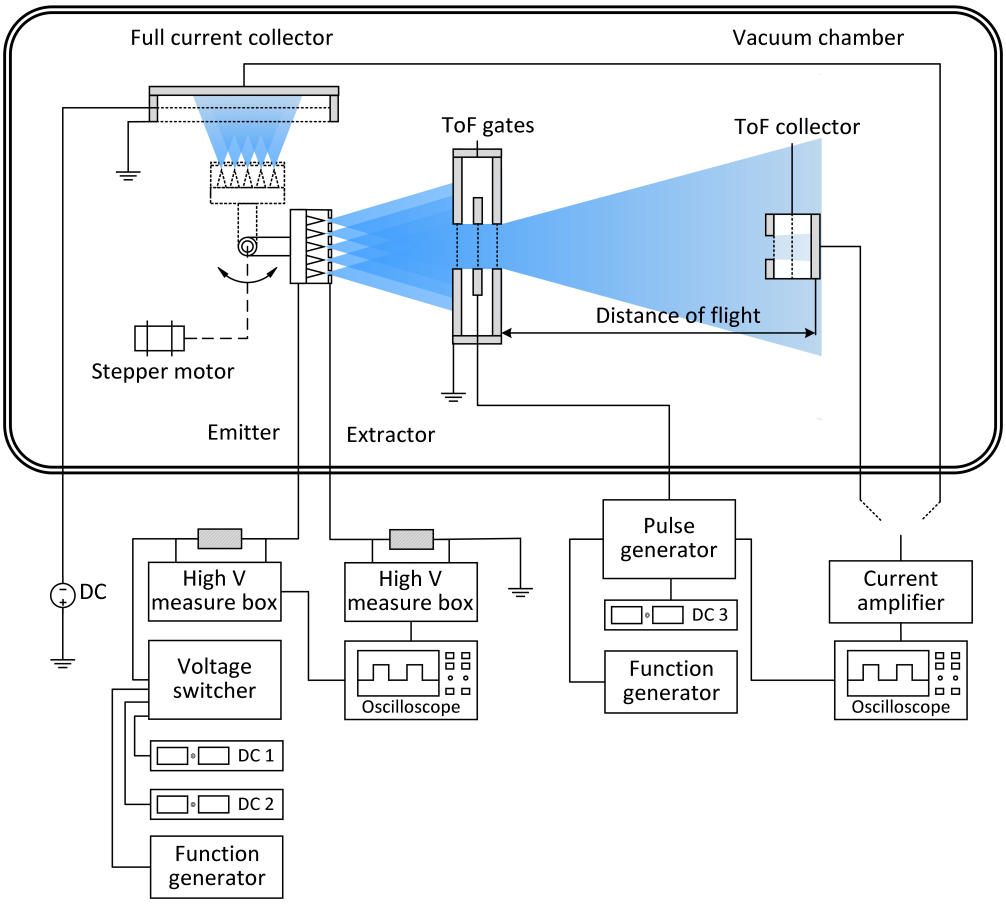

(a) Electrical system of the test set up.

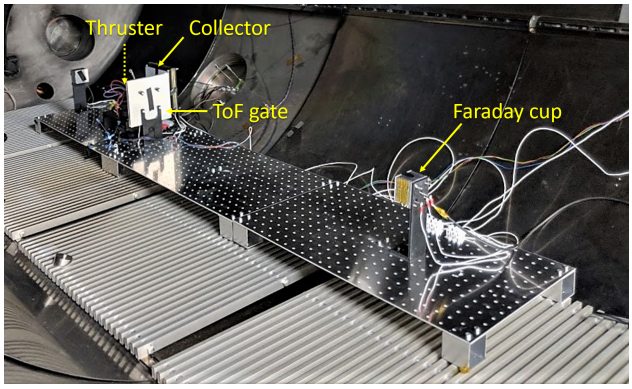

(b) Fully assembled test system.

Fig. 6 Illustration of the experimental system set up.

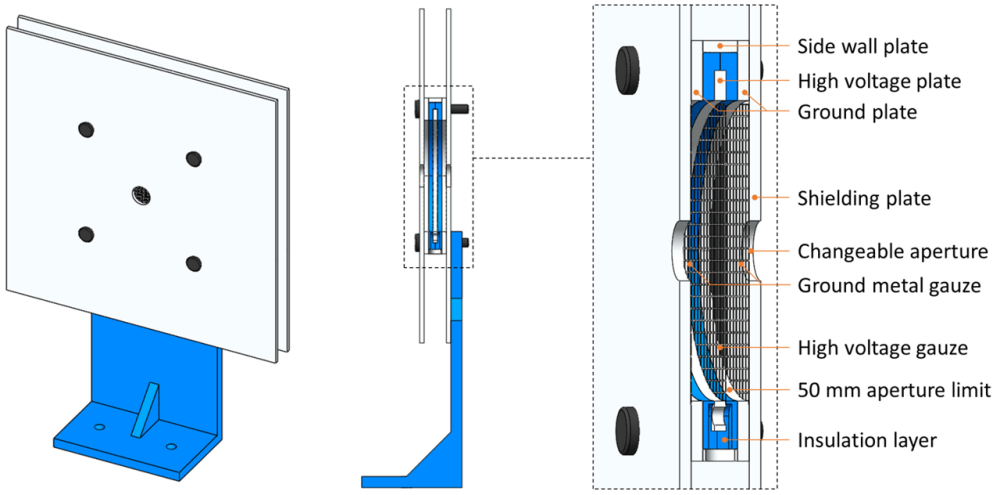

Fig. 7 Design of the time-of-fight gate.

B. Time-of-flight system

In order to measure the specific impulse and calculate the thrust, the species within the plume were characterized using a time-of-flight system, as illustrated in Figure 6. The ToF system discussed in this paper was built based on conventional ToF system designs that were utilized previously in electrospray thruster experiments [27, 29]. It contains a ToF gate and a downstream ToF collector, with the thruster operating upstream of the ToF gate. The function of this ToF gate is to impede the charged particles in the plume from reaching the collector. The ToF gate consists of three aluminum plates 5 mm apart, as illustrated in Figure 7. Each plate has a 10 mm diameter aperture covered with a nickel grid. The grids were sourced from Precision Eforming LLC, and have a transparency of 90% with a grid size of 344 μm and a wire width of 19 μm. The outer two ToF gate plates and grids were kept at ground potential, while the middle plate and grid were connected to a high voltage source, supplied by a PVX-4140 pulse generator from DEI Directed Energy, Inc. Upon receiving a command from a signal generator, the pulse generator can rapidly raise the output to a high voltage in less than 25 nanoseconds. The pulse generator has two inputs, with one kept at the ground potential while the other one connected to a FuG HCP 350-12500 high voltage source, which can output a voltage up to ±12,500 V with a 25 mA maximum current limit. The current received on the ToF collector is measured using a FEMTO DHPCA-100 current amplifier with an amplifying range from 10^2 to 10^8, and the amplified current was recorded using an oscilloscope, resulting in a ToF trace.

V. Thruster current-voltage characteristics

The thruster currents included emitter current, extractor current and emission current. The emitter current is the total thruster current passing through the emitter, including the total particle emission current and a small amount of propellant leak current to the extractor; the extractor current consists of the leak current and the current of the intercepted

charged particles on the extractor electrode; the emission current is the plume current that has exited the thruster. The relations of these current components are summarized as

$$I_{emt} = I_{ext} + I_{emi} \tag{1}$$

$$I_{ext} = I_{leak} + I_{emi-int} \tag{2}$$

$$I_{emi} = I_{emi-tot} - I_{emi-int} \tag{3}$$

where I_{emt} is the emitter current, I_{ext} is the extractor current, I_{leak} is the current loss due to minor fluidic leakage between the emitter and the extractor, and $I_{emi-tot}$, $I_{emi-int}$ and I_{emi} are the total electrospray emission current from the emission tips, the current of the emitted particles intercepted by the extractor, and the current of the plume exiting the thruster, respectively. Notably, only the emitter current, the extractor current and the plume current are measured in these tests, while the leak current and the intercepted emission current could not be distinguished.

A. Currents with Single-Tip Emitters

In the initial testings, pyramidal-shaped single-tip emitters with a side surface angle of 20 degrees were configured in the PET-100-MK1 thruster. The emitter and extractor current were calculated based on the ISO-TECH IDM 507 multimeters voltage readings on the serially connected measuring resistors. The extractor used had a 10×10 array of apertures, and each aperture had a diameter of 1.5 mm. The emitter tip was aligned to the centre of an aperture at column 5 and row 5. The alignment between the emitter-tip and aperture-centre was examined using an optical microscope, and the offset was usually below 100 μm with different single-tip emitters. This misalignment length could be considered relatively large when compared to many other micro-fabricated electrospray thrusters, such as the ion Electrospray Propulsion System (iEPS) using an extractor with an aperture diameter of 300 μm fabricated using micro-electromechanical systems [8]. However, as the PET-100-MK1 thruster extractor had a much larger diameter of 1.5 mm, the effects on the electric field distribution from the misalignment distance up to 100 μm is deemed negligible. In these initial thruster investigations, the alignments of the emitters and the extractor were deemed acceptable for conducting tests. The distance between the emitter tip and the extractor bottom surface was 1.2 mm. Multiple current-voltage measurements of this thruster configuration were conducted. With a bipolar frequency of 0.1 Hz, a typical curve of emitter current and extractor current variations over different voltages is shown in Figure 8.

The plume emission currents dicussed here were calculated as the difference between the emitter current and the extractor current, as shown in Equation 1. In this test, the multimeters measuring the resistor voltages were connected to a computer via infrared optical connectors. The measured data showed the emitter current and the extractor current fluctuated when applied with a constant voltage, based on the variation magnitudes, the error margins of these recorded current data were taken as 5 μA plus 10% of the measured values. In this test, the onset voltages at the two polarities

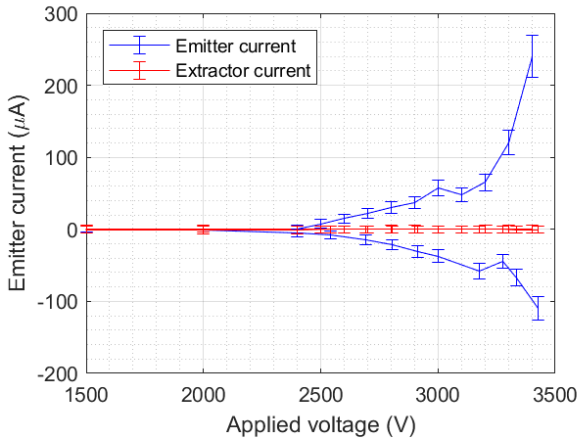

Fig. 8 Emitter current and voltage characteristics of the thruster using a single-tip P4 porous glass emitter and a P1 porous glass reservoir.

were approximately ±2400 V. The emission currents gradually increased with the applied voltage until it reached +3200 and -3277 V, where the emission currents were 64.1 and -45.6 μA. As the emitter voltage further increased to +3400 and -3425 V, the emitter currents were drastically increased to 240.5 and -110.1 μA.

In some of the other single-tip emitter tests, the extractor current significantly increases with the voltage applied. A possible explanation for the increase of extractor current proportion is that the thruster plume angle increases when operated at higher voltages. Consequently, an increasing proportion of the emitted charged particles were intercepted by the extractor electrode, and the intercepted particles would accumulate over time. As the thruster voltage increased to higher than ±3400 V, the extractor current was found to experience severely unstable current spikes. In post-test inspections, a ring of dark liquid surrounding the extractor aperture, suggesting droplets are present in the plume at these conditions. A probable reason for such unstable currents was that the deposited liquid accumulated liquid formed conductive paths between the emitter and the extractor, which caused the thruster shorting after a few minutes of operation.

These results suggested that the increase of the emission current becomes more rapid at higher voltages between the emitter and the extractor. Emission of droplets was suspected occurring at higher voltages, but this case was not certain at lower voltages, which needs to be confirmed with ToF measurements as discussed in Sect VI.A.

The post-test single-tip emitter was inspected, and the upper part of the porous emission tip was found covered and filled with dark-coloured substances, which were deemed as the products of the electrochemistry between the counterions in the propellant and the emitter materials. More of these substances were found with longer thruster operating time and higher emission currents, and they could block the propellant transport paths through the porous structure, affecting the electrospray emission performance. Therefore, these electrochemical effects are considered detrimental to the operation of the thruster and need to be mitigated to the greatest possible extent.

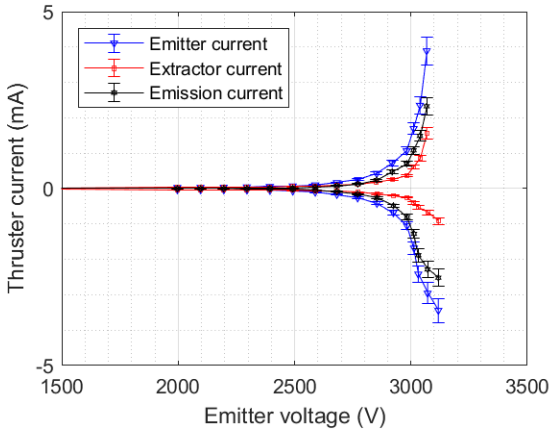

Fig. 9 Current-voltage characteristics of the PET-100-MK1 thruster using a P4 grade 25-tip emitter.

These tests of the PET-100-MK1 thruster using P4 grade single-tip emitters demonstrated that the thruster was able to achieve a considerably higher per-tip emission current than most other similar electrospray thrusters recently developed [8, 30].

B. Currents with 25-Tip Emitters

The emitter currents of 25-tip emitters were expected to be nearly 25 times higher than the single-tip emitters. Its emitter current was measured using a set of resistors with different electrical impedance connected in serial between the emitter and the power supply. The total electrical impedance of these resistors were 111.1 kΩ, and the resistor used to measure the emitter current in this test was 10 kΩ. Due to the high resistance of the measurement system, the voltage losses through these resistors from the increased emitter current cannot be neglected and the actual thruster voltage was therefore corrected. With proper liquid sealing and plume control design, the extractor current was expected to be low enough to be measured using only one 100 kΩ resistor, similar to the current measurement method in tests of single-tip emitters. The emission current was collected using a downstream collecting plate, whose data was then amplified and then recorded. The corrected current-voltage curves at a bipolar frequency of 0.117 Hz are shown in Figure 9.

The onset voltage of each emission tip could vary slightly due to their manufacturing geometric differences, such as in height and tip curvature radius. The starting onset emitter voltages were found ±2295 V with the lowest measurable emission currents of 1.96 and -1.89 μA. At +3067 and -3118 V, the maximum total emission currents were 2.33 and -2.52 mA, corresponding to the maximum emission current per tip of +93.2 μA and -100.8 μA, respectively. The electrospray current from each emission tip was not individually measured, but they were expected to have different values at the same voltage due to the geometric differences of these tips. The differences were also shown in the post-test inspection of the emitter, where some of the emission tips were covered with a larger area of and darker substances, suggesting that these tips had higher emission current and experienced more severe electrochemical effects compared to

the rest.

The maximum overall emission currents achieved by PET-100-MK1 thruster using a P4 grade 25-tip emitter were higher than most electrospray thrusters using similar designs being developed. For example, the nominal maximum current of the micro-fabricated iEPS thruster using a 480-tip emitter was around 200 μA [6, 8]. The BET-300-P thruster using CNC machined prism emitters demonstrated a maximum emission current around 800 μA[22]. A thruster using CNC machined emitter array, developed at Air Force Research Lab, produced ±700 μA of emission current at approximately ±1840 V [30].

The input electrical powers of the thruster at different voltages were corrected by excluding the power losses of the measuring resistors from the overall power supply output power. The minimum operational power was less than 0.1 W at ±2300 V, and the maximum bipolar power inputs of the thruster were 11.67 and 10.64 W required at +3067 and -3118 V.

C. Currents with 100-Tip Emitters

In an attempt to further increase the overall emission current, emitters with 100 emission tips were tested. The bipolar switching frequency was increased to 1 Hz to mitigate the electrochemical effects more effectively.

1. P4 grade emitter

A P4 porosity grade 100 tip emitter was tested with the extractor placed 0.5 mm above the emitter tips. The extractor used had 1 mm-diameter apertures. The current-voltage curves of the emitter and the extractor are shown in Figure 10, with the 0 mm and 0.5 mm indicating the mean distances between the emitter tips to the upstream surface of the extractor. At high voltages, the extractor current was relatively large compared to the emitter current, of which the ratios are shown in Figure 1. The ratios are relatively low before ±1900 V, as the emitter current was mostly made of the extractor current, generated mainly via minor conductive paths in between. At ±3500 V, the extractor current is about 13.5% to 33.5% of the emitter current, and the thruster stopped working after approximately 10 minutes. For this PET-100-MK1 thruster configuration, the plume half-angle threshold of the plume interception by the extractor is approximately 45 degrees. A plume with a half-angle beyond 45 degrees will lead to the gradual accumulation of the emitted particles on the extractor surface. if the plume only contains high-energy ions, it will gradually erode away the electrode material; or, if the plume contains droplets, the accumulated particles will gradually form a conductive liquid path and result in short circuit and thruster failure. As either result was detrimental to the thruster operation, it was deemed that the high voltages near ±3500 V could not be categorized to the suitable operation range of this thruster configuration due to its large plume angle. In such scenarios where the plume angle exceeds the threshold for extractor intercepting particles, the current-voltage point measurements were all done within 20 seconds, well before thruster shorting.

The collected emission current-voltage curve of this thruster is shown in Figure 11. The onset voltages were ±2200 V, and at ±2300 V the emission currents were ±40 μA. The maximum emission currents were +3.22 mA and -4.72 mA

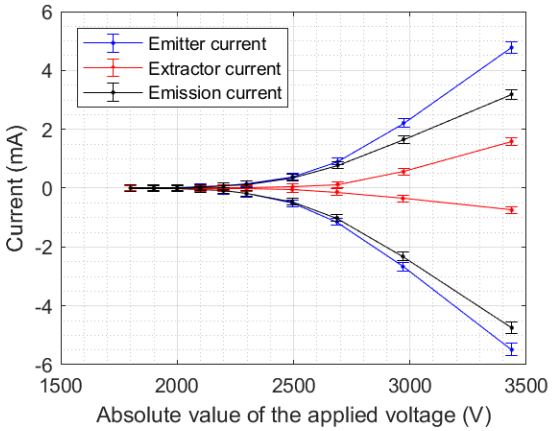

Fig. 10 Emitter, extractor and emission current curves of the PET-100-MK1 thruster using a P4 grade 100-tip emitter at different thruster configurations.

Table 1 The ratios of the emission current compared to the emitter current at different thruster voltages.

V_{pos} (V)	I_{emi}/I_{emt}	V_{neg} (V)	I_{emi}/I_{emt}
1799.9	0.3333	-1799.9	0.2609
1899.8	0.8367	-1899.8	0.6293
1999.7	0.8333	-1999.8	0.6954
2099.5	0.8102	-2099.6	0.8262
2199.0	0.9283	-2199.2	0.8839
2297.9	0.9212	-2298.4	0.9049
2494.3	0.8958	-2495.7	0.8975
2687.2	0.8844	-2689.7	0.8619
2969.8	0.8687	-2972.4	0.7491
3437.6	0.8642	-3436.4	0.6675

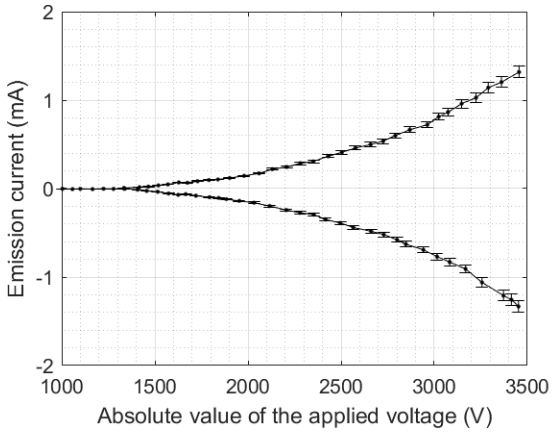

Fig. 11 Emission current of the PET-100-MK1 thruster using the P5 grade 100-tip emitters.

achieved at ±3500 V, respectively.

2. P5 grade emitter

The PET-100-MK1 thruster was also tested with a P5 grade 100-tip emitter and zero distance between the emitter tips and the extractor upstream surface. The P5 emitter had slightly sharper emission tips, whilst other thruster configurations were kept the same. A full emission current collector was used to collect its total emission current, with the results shown in Figure 11. During this test, the emitter voltage polarity switching frequency was 1 Hz. Each HCP 35-3500 power supply was integrated with a stepper motor on its voltage controller, making them programmable using an Arduino Uno board. Therefore the current-voltage curves of PET-100-MK1 using P5 emitters were automatically collected using a sweeping program.

The onset voltage of this thruster was approximately 1400 V, which was considerably lower than the minimum operating voltage of 1800 V when using the P4 emitter, possibly because the sharper tips of the P5 grade emitter can concentrate the electric field more effectively and can reach the critical electric field strength for emission at a lower voltage. However, the overall emission current of the P5 grade emitter is lower than P4 grade emitters at higher voltages. For example, at ±2800 V, the emission current of the P5 grade emitter is about ±0.53 mA, which is only about 1/5 of the corresponding P4 grade emitter emission current. The relatively lower emission current at high voltages of the P5 grade emitter is suspected to be a result of its sharper tip geometry, which possibly leads to a smaller area for emission than the P4 grade. Another possible explanation lies in the differences in propellant flow rates, which were significantly affected by the hydraulic impedance of the thruster. The average pore size of the P5 grade emitter was roughly one-tenth of the P4 material, which would significantly increase the hydraulic impedance of the material. In the PET-100-MK1 thruster design, the electrospray emission is a result of excessive electrical stress extracting charged particles from the porous material, therefore a higher hydraulic impedance would significantly limit the flow rate and the emission current.

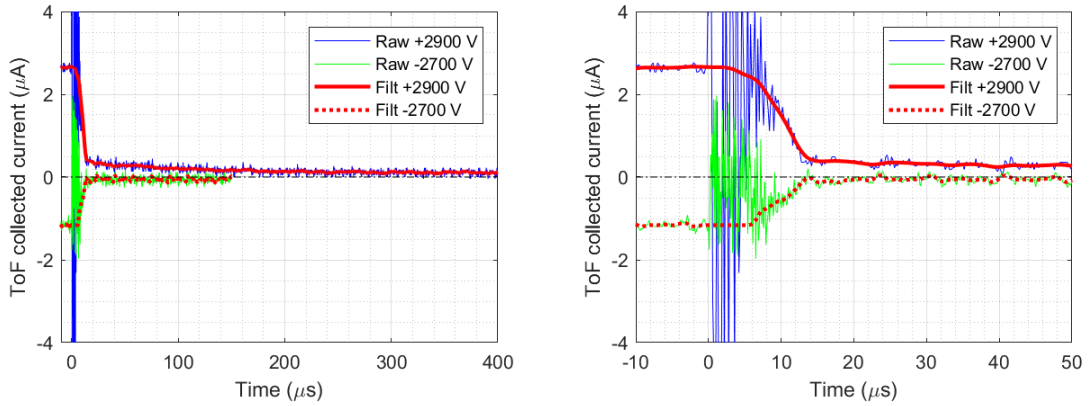

(a) Collected ToF data and filtered data curve.

(b) Zoomed-in figure near the major current-decrease section.

Fig. 12 Collected and filtered ToF data of a single-tip emitter at two different polarity voltages.

VI. Time-of-flight characterization

Time-of-flight measurements were done with the thruster using single-tip emitters, 25-tip emitters and 100-tip emitters, and the results are discussed in this section.

A. ToF results of a P4 grade single-tip emitter

Single-tip P4 grade emitters were tested first using a ToF system with the initial design. The emitter had a side surface angle of 20 degrees with a P3 grade reservoir, which had a nominal maximum pore size of approximately 16 to 40 μm. The ToF gate consisted of three layers of aluminium plates with a adjacent distance of 2 mm, with the front plate placed 2 mm from the thruster extractor sheet. The ToF collector in these single-tip emitter tests was a 37 mm square aluminium plate without any charged metal grid in front of it. The distance between the ToF gate back plate and the ToF collector was 55 cm. Two typical ToF traces of the thruster using a single-tip emitter are shown in Figure 12, where the the emitter potential was +2900 V and -2700 V. As the collected currents had drastic variations around 10 μs, a zoomed-in figure is also presented showing the currents from -10 μs before the ToF gate voltage triggering to 50 μs after the triggering.

The blue and green curves represent the raw data of the current collected at +2900 V and -2700 V, respectively. Notably, the collected ToF current experienced significant inductive current noises as the ToF voltage switched on, and the noises lasted for approximately 7 to 12 μs. The red curves in these two figures are filtered and corrected current data. Multiple Gaussian filters and Butterworth filters were attempted in the ToF current data filtering, yielding results with little distinguishable features where the time scale is larger than 12 μs. However, from 0 to 12 μs, the inductive current noises exceeded the measurement range of the oscilloscope at times, and the lost data would make these filtering techniques generate implausible current features. Therefore, additional data processing procedures were applied. As the ToF current should never significantly exceed the readings near 0 s, this initial current value was maintained and

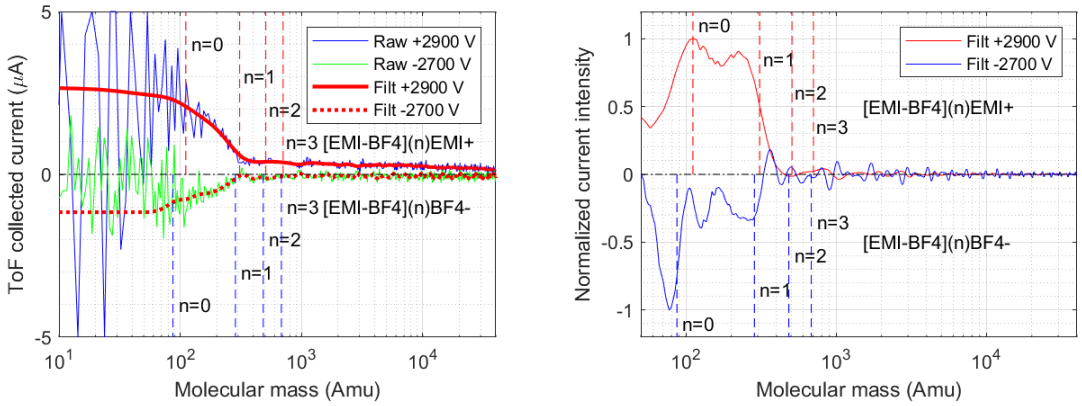

(a) ToF current vs. molecular mass.

(b) Normalized current intensity.

Fig. 13 Calculated molecular mass distribution of a single-tip emitter at positive and negative voltages.

extended to the arrival time of the fastest possible species in the plume, monomer ions, to the ToF collector.

The theoretical time-of-flight of a charged particle in the plume can be calculated by

$$t = \sqrt{\frac{L^2}{2V_{ac}}\frac{m}{q}}. \tag{4}$$

The mass of a positive dimer ion, EMI-BF_4)EMI^+, is 309 Amu. Assuming there is no voltage loss during the ion extraction, its theoretical time-of-flight is 20.7 μs at +2900 V, which is already longer than the largest current variation end time around as shown in 12, indicating that the thruster was operated in highly or purely ionic emission regime. It is safe to assume that all the emitted particles were singly charged in a purely ionic emission regime. Thus, the time axis in Figure 12 can be replaced by the molecular mass, *Amu*, as shown in Figure 13(a).

The ToF current curves at +2900 V and -2700 V demonstrated significant current drops between 6 to 12 μs, and in the curves using molecular mass axis these drops are within the mass range of dimer ions. The negative current reached 0 μA after 12 μs and had no further drop of the ToF collector current within 400 μs, suggesting that all negatively charged particles had reached the collector by 12 μs, demonstrating that the emitted particles at -2700 V were all monomer and dimer ions. In comparison, the positive current demonstrated a slow and gradual drop, however, without any rapid current change, from 12 μs to about 250 μs, corresponding to a molecular mass range from 400 to more than 4×10^4 Amu. This part of gradual current decrease over time could result from the presence of species in the plume that are heavier than dimer ions, or, it could be errors from the measurement instrument system.

In order to identify the dominant source causing the gradual current variation, the ToF current in the curve of molecular mass was converted to the normalized current intensity. The local slopes of y-axis ToF current data in Figure 13(a) was calculated by taking the gradients between any two adjacent points on the filtered current curve. These local

slope data were then normalized with a standard deviation of 1, representing the normalized current intensity over different molecular masses, which were then plotted in Figure 13(b). Figure 13(b) clearly shows the relative current intensity of charged particles of different masses. Evidence of monomer and dimer ions is the dominant current in these curves. The results of the -2700 V case supported the statement that the single-tip emitter achieved purely ionic emission under such conditions. However, the ToF current curve at +2900 V, where a slight and gradual decrease is present from 400 to more than 4×10^4 Amu in Figure 13(a), does not show obvious values over this mass range in Figure 13(b). In the case that this gradual current decrease was resulted from the emission of heavier species, such as droplets, the current intensity results suggests that these particles have a evenly but widely distributed low-density values of specific charges.

B. ToF results of a P4 grade 25-tip emitter

As the ToF results of the single-tip P4 emitter demonstrated promising results with highly ionic emissions, in the next ToF measurements a 25-tip emitter wsa tested. The 25-tip emitter was made of P4 grade porous borosilicate material, and its geometrical features were discussed in subsection III.A. The ToF system was updated in these tests. The ToF gate was placed 50 mm away from thruster extractor to reduce close-range interaction of sputtered particles, and the size of the grounded aluminium plates in the ToF gate was increased to 150×150 mm to block particles from passing from the ToF gate edges with the increased gap distance between the thruster and the ToF gate. In attempts to reduce the inductive current caused by the pulsed electric field at the moment when the ToF gate voltage is switched on, the size of the ToF collector was reduced to 37 mm square, and the distance between the ToF collector and the ToF gate was increased to 90 cm, however, at the expense of reducing the currents collected. Noticeably, no electrically charged mesh was placed just upstream of the ToF collector plate. The ToF measurment results at the emitter-to-extractor voltages of +3067 V and -2771 V, corrected for the voltage losses through the measuring resistors in both the emitter line and the extractor line, are shown in Figure 14(a), with the plume emission currents of 2.325 mA and -156 μA, respectively.

The positive ToF current of the 25-tip emitter had a smooth and major drop from 9 to 12 μs, corresponding well to the theoretical arrival time of monomer positive ions. However, the negative ToF current lost a certain amount of fidelity due to current oscillation caused by significant noises. As a result, the calculated initial major negative current decrease occurred slightly earlier than the theoretical arrival time of the negative monomer ions, resulting in a lighter current intensity peak in Figure 14(b). The inductive current noises also caused current fluctuations on the negative current, which turned positive around 10 μs and returned to near-zero values around 14 μs. Then the signal had a negative current offset between 20 and 40 μs, which returned to near-zero values after 40 μs. Despite the signal variations on the received negative current, the ToF results of the P4 grade 25-tip emitter demonstrated a highly ionic emission containing almost pure monomer ions at +3500 V and -2800 V.

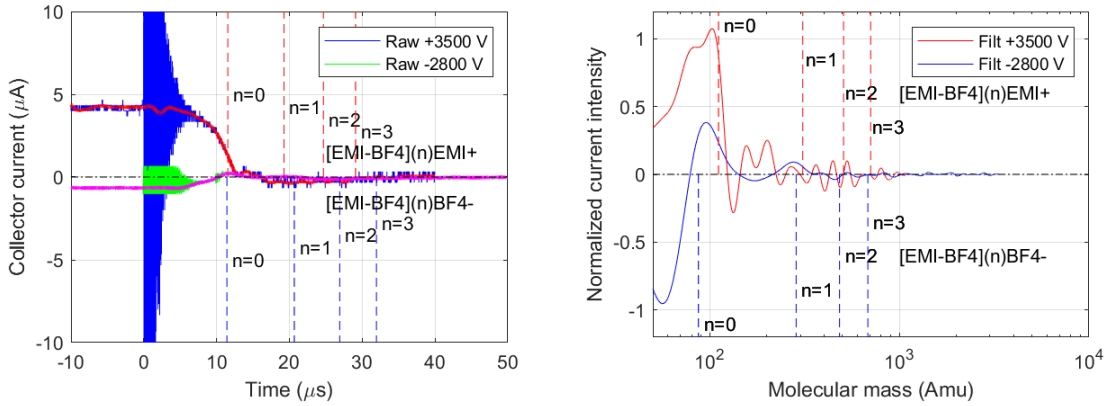

(a) Collected ToF raw data and filtered data curves.

(b) Normalized current intensity.

Fig. 14 Collected and filtered ToF data of a 25-tip emitter at different positive and negative voltages.

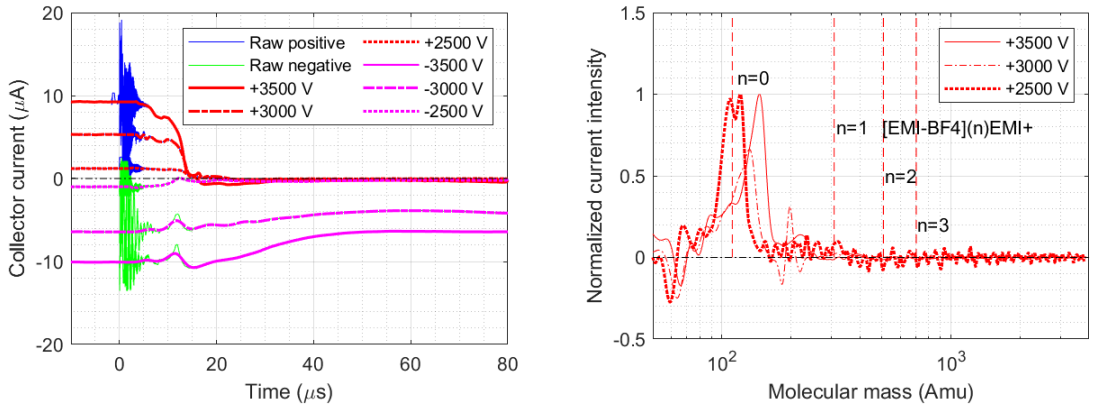

(a) ToF traces raw data and Gaussian filtered results.

(b) Normalized current intensity distributions.

Fig. 15 ToF traces and plume compositions of a 100 emitter array using P4 emitter at different positive and negative voltages.

C. ToF results of a P4 grade 100-tip emitter

Using the same ToF system set-up as the 25-tip emitter, a P4 grade 100 tip emitter was then characterized. The thruster operated at a bipolar mode with an polarity-alternating frequency of 1 Hz. The ToF characterization results of the PET-100-MK1 with a P4 grade emitter at different voltages are shown in Figure 15.

The corrected emitter-to-extractor voltages at the applied potentials of +2500 V, +3000 V and +3500 V were *******, with the directly measured plume currents of +350.1 μA, +1.656 mA and +3.188 mA, respectively. The ToF measurements at these voltages had smooth and drastic current decreases near the theoretical arrival times of monomer ions, which are considered as the majority of the plume particles within the range of these positive voltages. The current fluctuations suggest that there probably were some heavier species, dimer ions, in the plume; however, these were in minor proportions that appeared to be negligible.

In comparison, the negative ToF curves experienced different trends at different negative voltages. At the applied voltages of -2500 V, -3000 V and -3500 V, the corrected emitter-to-extractor voltages were *****, with the plume emission currents of -460 μA, -2.32 mA and -4.746 mA, respectively. At -2500 V, the negative ToF current decreased in a similar way as the current curves at positive voltages, reaching close-to-zero values near the arrival time of monomer ions. However, at -3000 V and -3500 V, although the current curves did had noticeable decreases within 60 μs, they did not decrease to near-zero values within the total recording time of 400 μs. A possible reason was that there were heavier droplets contained in the emitted particles, and the total measurement time was not long enough to record their arrival time. The specific charge of a droplet varies in a range because its mass and the number of charges are not certain. The molecular mass distribution figures of the ToF results are usually plotted assuming all the particle are singly charged for the purpose of showing the current intensity of light-mass ions, including monomer, dimer and trimer ions. Therefore, these molecular mass distributions can be easily converted to illustrate the distributions of the specific charge. In other electrospray thruster studies that found evidence of droplets in the plume when using EMI-BF_4 propellant, the lowest specific charge usually goes down to the level from 3000 C/kg [16] to 90000 C/kg [27]. In this study, the theoretical specific charge at 400 μs under 3500 V with 0.9 m distance between the ToF gate and the collector is approximately 723 C/kg. As the ToF current values remained relatively high above zero at 400 μs, these postulated droplets would have even lower specific charges that have not been observed in other electrospray thrusters with similar designs. It is also possible that these residual negative currents came from unidentified instrumentation errors. The reasons of the ToF measurement differences between positive voltages and negative voltages are unclear. As these two negative current curves did not complete by reaching near-zero values, they were not used in further performance analysis.

D. ToF results of a P5 grade 100-tip emitter

In an attempt to reduce the signal noises induced by the pulsed electric field in the following ToF measurements of the P5 grade 100-tip emitter, a Faraday cup was built and used to replace the previous flat plate ToF collector. The Faraday cup consisted of an aluminium collector, a negatively charged grid, a grounded grid and grounded shielding walls. The negatively charged grid was kept at -30 V and placed before the collecting plate, primarily to suppress secondary electrons emitted from the collision of high-energy particles on the ToF collector plate. The grounded grid in its front is to maintain the non-acceleration region between the ToF gate and the ToF collector. In addition, an aluminium square tube was connected between the ToF gate and collector, to avoid particles spreading after leaving the ToF gate. Therefore, the risk that the spreading high-energy particles colliding on the vacuum chamber steel wall and generating secondary electrons became less probable. Using this upgraded ToF system, the ToF traces of the PET-100-MK1 using the P5 emitter are shown in Figure 15.

The collected plume emission currents at +2400 V, +2800 V, +3000 V, -2000 V, -2200 V and -2600 V were +345.2 μA, +610.5 μA, +781.2 μA, -151.9 μA, -242.1 μA and -454.6 μA, respectively. The results showed that signal noises

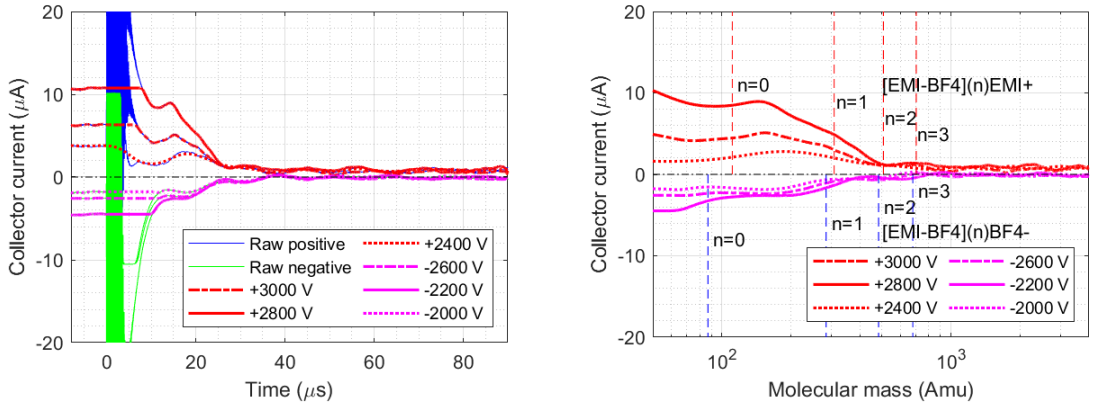

(a) ToF traces raw data and Gaussian filtered results.

(b) Specific charge and molecular mass distribution.

Fig. 16 ToF traces and plume compositions of a 100 emitter array with P5 emitters.

induced by the pulsed electric field were not suppressed effectively by the Faraday cup current collector. These ToF traces suggest that highly ionic emissions were achieved at positive voltages from +2400 V to +3000 V and negative voltages from -2000 V to -2600 V. Most of the current decayed within the theoretical flight time of dimer ions. Figure 16(a) shows all the negative current curves reached near-zero values around 35 μs, but the positive ToF traces still have about 0.8 μA of current left after 50 μs. The positive residual currents had similar features to the ToF measure of the single-tip emitter at +2900 V within the first 90 μs of the measurements, but these currents remained a stable trend and did not show signs of converging to zero over the 400 μs of total recorded time. Another feature is that these residual signals showed extremely close current levels, despite that their initial currents at 0 s were significantly different. To conclude, the residual positive currents are deemed more likely resulted from instrumentation errors that have not yet been identified, compared to the possibility of uncommonly heavy droplets being present in the plume.

The distributions of the molecular mass assuming all particles are singly charged are shown in Figure 16(b). Compared to the previous ToF testing results on P4 emitters, the slope of these ToF current curves are less steep. This was probably a result of the fragmentation of heavier species, dimer ions, into lighter species, monomer ions [31]. When the fragmentation process occurs during the acceleration stage, the lighter charged particles after the fragmentation would gain a higher velocity than dimer ions but still less than that of monomer ions, resulting in a spread distribution of arrival time of particles to the collector.

E. ToF results summary

Signal noises induced by the pulsed elcetric field from the operation of the ToF gate were found the major issue affecting the analysis of the ToF measuremenrs. Multiple methods were attempted to reduce the effect, including increasing the distance between the ToF gate and ToF collector, reducing the size of the ToF collector, ground shielding

the ToF gate and replacing the flat plate collector with a Faraday cup, but the noises could not completely reduced. A systematic diagnosis on the measurement system will be done in a future test in order to suppress the noises effectively. Nonetheless, the signals were only masked by such noises within a short duration, and the ToF measurement results in this study still provide strong supports that purely ionic emissions were achieved using EMI-BF_4 propellant at certain thruster operation conditions, including P4-single-tip emitter at -2700 V, P4-25-tip emitter at -2800 V and +3500 V, P4-100-tip emitter at +2500 V, +3000 V and +3500 V and P5-100-tip emitter at -2000 V, -2200 V and -2600 V. In some other conditions, residual currents over a longer period of time were found. The residual current of P4-single-tip emitter at +2900 V gradually returned to zero, suggesting that this is likely to be a result of droplets contained in the plume. However, the residual currents of P4-100-tip emitter at -2500 V, -3000 V and -3500 V and P5-100-tip emitter at +2400 V, +2600 V and +3000 V did not show signs of converging to zero over a reasonably long period of time, hence, it is uncertain whether these were results of droplets with lower specific charge in the plume, or were results of instrumentation errors that need further work to be identified.

The purely ionic emissions found in these tests are suspected a result of the high fluidic impedance of the thick emitters, which has a base thickness of 5 mm and a tip height of 2 mm. In comparison, another highly ionic emission electrospray thruster using P5 grade 3 mm thick CNC machined prism emitters, on which this paper was based, had emitter prism heights of approximately 350 μm [27]. This thruster achieved approximately 95% ionic emission including trimer ions, and the remainder of the current indicated the presence of heavier species up to 800 Amu. Other studies demonstrated that when using thinner porous emitters, droplets are often present in the plume. For example, a porous glass emitter with a tip height of 160 to 175 μm demonstrated ToF traces that approximately 90% of the plume current was resulted from species lighter than (EMI-BF_4)$_3$$EMI^+$ or (EMI-BF_4)$_3$$BF_4^-$, while the other 10% current represented heavier species with a mass around 10^4 Amu [16].

VII. Thruster performance Estimation

The time-of-flight traces indicate the velocity, mass and current proportion of the plume particles, which can be used to estimate the thruster performance. However, only completed ToF traces, which return to the zero value and shows information of all the particles in the collected plume, can be used for such estimation, including P4-single-tip emitter at -2700 V, P4-25-tip emitter at +3500 V, P4-100-tip emitter at +2500 V, +3000 V and +3500 V and P5-100-tip emitter at -2000 V, -2200 V and -2600 V. The thruster performance in these purely ionic emission cases, which are summarized in Figure 17, is calculated in this section. It should be noted that the thruster showed evidence of droplets emission at certain conditions, which would result in drastic variations on the thrust and specific impulse. However, as their corresponding ToF traces were not completed over the total measurement time, these are not discussed in this section.

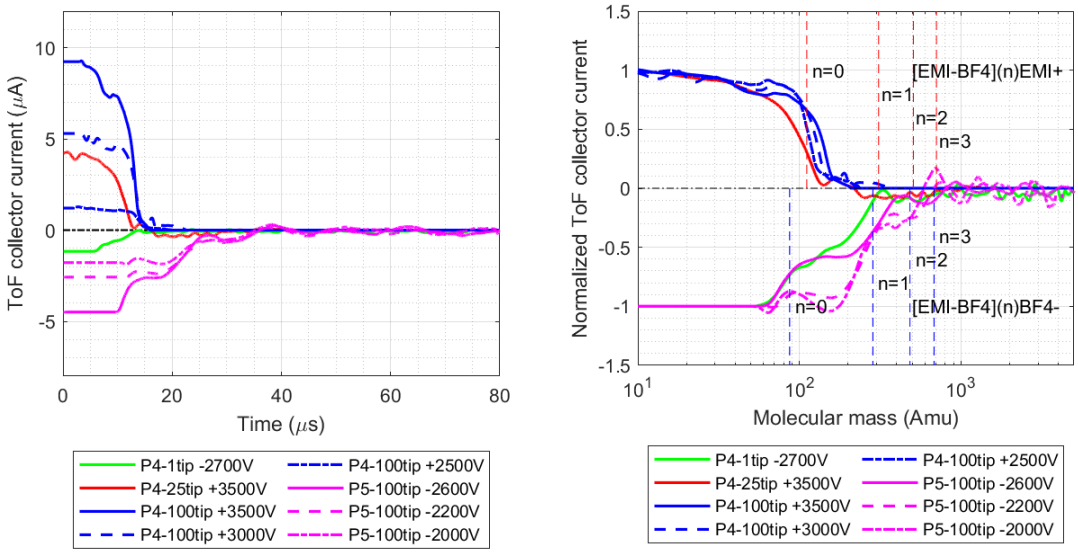

(a) ToF traces that demonstrate purely ionic emissions.

(b) Molecular mass distribution of the ToF traces with the current magnitude normalized.

Fig. 17 Summary of normalized ToF measurement results using different emitters and thruster configurations.

A. Unidirectional Performance for Per micro-ampere Plume Current

All the grids used in this study were 90% transparent, as a result the collected current need to be corrected by applying an amplifier of 1.11 for each grid it had before its collecting plate. The mass flow rate received on the ToF collector can be calculated from a ToF trace, based on

$$\dot{m}_t = \frac{4V_{ac}}{L^2}\int_0^\infty I(t)t\mathrm{d}t, \tag{5}$$

where V_{ac} is the particles acceleration voltage, L is flight length between the ToF gate to the ToF collector, t is the time and $I(t)$ is the current variation over time. Assuming that the plume composition does not vary radially, the overall mass flow rates of the emission can be calculated based on the ratio of received current on ToF collector compared to the overall emission current. In order to understand the propulsive performance for per unit current of the plume, the calculated total mass flow rates from ToF traces are divided by the initial current collected on the ToF collector, and the results are shown in Table 2. As comparison, theoretical performance of purely monomer ions emission and purely dimer ions emission are shown in brackets in the table.

$$\dot{m}_{th} = \frac{Im}{q}. \tag{6}$$

Table 2 Estimated mass flow rates, thrust and specific impulse of the PET-100-MK1 thruster for per-unit of plume current.

Configuration -	$V_{applied}$ (V) V	I_t μA	$\dot{m}_t$ (mono/di) $10^{-3} \times \mu$g/(s·μA)	T_t (mono/di) $10^{-2} \times \mu$N/μA	Isp_t (mono/di) (s)
P4-1-tip	-2700	-1.163	1.87(0.90/2.94)	8.9(6.6/11.9)	4856(7483/4130)
P4-25-tip	+3500	+4.252	1.16(1.15/3.19)	6.4(8.5/14.2)	5629(7542/4542)
P4-100-tip	+2500	+1.206	1.12(1.15/3.19)	6.8(7.2/12.0)	6195(6387/3839)
P4-100-tip	+3000	+5.299	1.13(1.15/3.19)	7.5(7.9/13.1)	6773(7010/4190)
P4-100-tip	+3500	+9.233	1.10(1.15/3.19)	8.0(8.5/14.2)	7421(7542/4542)
P5-100-tip	-2000	-1.779	2.56(0.90/2.94)	9.4(5.7/10.3)	3703(6463/3575)
P5-100-tip	-2200	-2.574	2.55(0.90/2.94)	9.8(6.0/10.8)	3922(6803/3748)
P5-100-tip	-2600	-4.492	2.05(0.90/2.94)	9.3(6.6/11.7)	4629(7483/4061)

The thrust received on the ToF collector can be calculated based on

$$T_t = \frac{2V_{ac}}{L} \int_0^\infty I(t)\mathrm{d}t. \tag{7}$$

The theoretical thrust values from emissions of pure monomer ions and dimer ions can be calculated as

$$T_{th} = I\sqrt{\frac{2mV_{ac}}{q}}. \tag{8}$$

With the mass flow rate and thrust equations, the specific impulse can be calculated as

$$Isp_t = \frac{T_t}{\dot{m}_t g_0} = \frac{2L}{g_0} \frac{\int_0^\infty I(t)\mathrm{d}t}{\int_0^\infty I(t)t\mathrm{d}t}, \tag{9}$$

where g_0 is the Earth gravitational acceleration constant. Assuming 100% total efficiency, the theoretical specific impulse values of pure monomer ion emission and dimer ion emission can be calculated as

$$Isp_{th} = \frac{1}{g_0}\sqrt{\frac{2qV_{ac}}{m}}. \tag{10}$$

B. Propulsive Performance of PET-100-MK1 Thrusters

The total thrust can be estimated from the a ToF trace through integrating the effective propulsive forces along all plume directions, expressed as

$$T = \iint T_t(\theta_x, \theta_y)\cos\theta_x \cos\theta_y \mathrm{d}\theta_x \mathrm{d}\theta_y. \tag{11}$$

Table 3 Estimated propulsive performance at different PET-100-MK1 thruster configurations.

Configuration -	$V_{applied}$ (V) V	I_{emi} μA	$\dot{m}$ (mono/di) μg/s	T (mono/di) μN	Isp (mono/di) s
P4-1-tip	-2700	-21	0.003927(0.00189/0.006174)	1.495(1.109/1.999)	3885(6066/3304)
P4-25-tip	+3500	+2325	2.70(2.67/7.42)	119.0(158.1/264.1)	4503(6034/3634)
P4-100-tip	+2500	+350.1	0.39(0.40/1.12)	19.0 (20.2/33.6)	4956(5110/3071)
P4-100-tip	+3000	+1656	1.87(1.90/5.28)	99.4(104.7/173.5)	5418(5608/3352)
P4-100-tip	+3500	+3188	3.51(3.67/10.17)	204.0(216.8/362.1)	5937(6034/3634)
P5-100-tip	-2000	-151.9	0.39(0.14/0.45)	11.4(6.9/12.5)	2962(5170/2860)
P5-100-tip	-2200	-242.1	0.62(0.22/0.71)	19.0(11.6/26.1)	3137(5442/2998)
P5-100-tip	-2600	-454.6	0.93(0.41/1.34)	33.8(24.0/42.6)	3623(5936/3249)

where T is the overall thrust, θ_x and θ_y are the two perpendicular angles of the particle flying vector relative to the overall thrust vector and $T_t(\theta_x, \theta_y)$ is the thrust component produced by the flying particles along the (θ_x, θ_y) direction. However, as the angular characteristics of the plume were not directly measured in this study, this paper uses the measurement data of another electrospray thrusters using porous emitter arrays for performance estimation, with a plume half angle of 60 degrees and an angular efficiency around 80% [16]. The theoretical and estimated thrust values of the PET-100-MK1 thruster using the P4 grade 100 tip emitter at different voltages are shown in Table 3.

The estimated thrust of the single-tip emitter at +2700 V was approximately 1.5 μN. In comparison, with a maximum measurement voltage of ±3000 V, the thruster using the P5 grade 100 tip emitter achieved a thrust from 11.4 to 33.8 μN at negative voltages, whilst the thruster using the P4-100-tip emitter achieved a thrust from 19 to 204 μN at positive voltages. These results suggest that one emitter tip can achieve a maximum thrust of around 2.04 μN, which is relatively high compared to other electrospray thrusters. For example, a porous emitter array consisting of 480 tips achieved a total thrust of 12.5 μN, corresponding to 26 nN per emitter tip [16]. In order to estimate the total thrust more realistically, the thrust calculated from ToF traces needs to be integrated from all directions in the plume, therefore, the plume current density angular distribution need to be measured in the future.

The formula to calculate the total thruster specific impulse is the same as in the per-unit plume current calculation as in Equation 9. The specific impulse of the PET-100-MK1 thruster using a P4 grade 100-tip emitter is shown in Table 3, varying from 4500 s at +2000 V to more than 7500 s at +3500 V. For the P5 grade 100-tip emitter, the calculated specific impulse varies from 4375 s at +2200 V to 4790 s at +3000 V, and from 3900 s at -2000 V to 4800 s at -2600 V.

In the current thruster configuration design, the maximum size of the reservoir is $3 \times 3 \times 1$ cm. Given that the porous reservoir has a void ratio of approximately 50%, it can store up to 5.823 g of EMI-BF_4 propellant with the density of 1.294 g/mL at 25 $^\circ C$. The maximum mass flow rate of the thruster using the P4 grade emitter is 4.0 μg/s when the applied voltage is +3500 V, resulting in 404 hours of continuous operation with the maximum propellant storage. For the thruster using the P5 grade emitter, the maximum mass flow rate is 1.8 μg/s at +3000 V, which theoretically allows

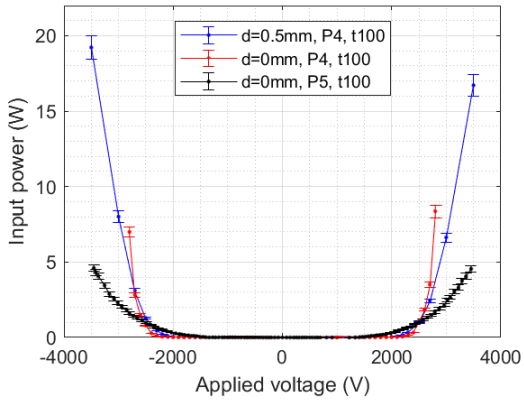

Fig. 18 Input power of PET-100-Mk1 thruster using 100-tip emitters.

899 hours of continuous emission. Noticeably, the thickness, and thus volume, of the reservoirs can be increased or reduced based on mission requirements. As the pore size of the P0 grade porous reservoir is about 100 times larger than that of P5 grade emitter material, changing the thickness of the reservoir would bring little influences on the hydraulic impedance, thus the thruster propulsive performance.

C. Efficiency components estimation

The total efficiency of the thruster can be obtained through comparing the jet power, P_{jet}, to the input power, P_{in}. The input power is calculated using the emitter current times the voltage between the emitter and the extractor, without taking the outside power loss such as the serial-connected resistors for current measurement. The input power values at different voltages are shown in Figure 18. The thruster can start working at a power around 0.2 W, and the maximum power of the PET-100-MK1 thruster was from 13.9 to 15.7 W at ±3500 V using a P4 grade 100 tip emitter with a emitter-extractor distance of 0.5 mm.

The primary components contributing to the total efficiency of an electrospray thruster can be expressed as [32]

$$\eta_0 = \frac{P_{jet}}{P_{in}} = \eta_{nk}\eta_i\eta_{tr}^2\eta_{ang}\eta_{poly}, \tag{12}$$

where η_0 is the total efficiency, η_{nk} is the non-kinetic efficiency, η_i is the ionization efficiency, η_{tr} is the transmission efficiency, η_{ang} is the angular efficiency and η_{poly} is the polydispersive efficiency. However, this study of current-voltage and ToF characterization can only illustrate transmission efficiency and polydispersive efficiency.

The polydispersive efficiency is resulted from species carrying different specific charges in the plume. If the plume contains two types of species, the polydispersive efficiency can be calculated from the current and mass ratios of each

Table 4 Efficiency components of the PET-100-MK1 thruster.

Configuration	$V_{emitter}$	η_{tr}	η_{poly}
P4-100-tip	+2500	0.8975	0.8613
P4-100-tip	+3000	0.7491	0.9171
P4-100-tip	+3500	0.6675	0.9452
P5-100-tip	-2000	0.9686	0.9377
P5-100-tip	-2200	0.9592	0.9349
P5-100-tip	-2600	0.9338	0.9275

specie illustrated in the ToF traces, based on [33]

$$\eta_{poly} = \frac{[1-(1-\sqrt{\omega})f_l]^2}{1-(1-\omega)f_l}, \tag{13}$$

where $\omega = \frac{(q/m)_h}{(q/m)_l}$ is the specific charge ratio of heavier to light species and $f_l = \frac{I_l}{I_l+I_h}$ is the fraction of ToF collected current ratio representing the light species. For example, the PET-100-MK1 thruster using the P4 grade 100 tip emitter, the +3000 V ToF traces suggests that approximated 91.3% of the current resulted from monomer ions and the other 8.7% of the ToF current represented dimer ions, leading to a ω = 2.78 and a f_l=0.91, resulting in a η_{poly}=0.986. However, in some ToF traces that contain more than two species as well as some fragmentation effects, such as the ToF traces using P5 grade emitters as shown in Figure 16, the equation 13 cannot be easily applied to calculated the polydispersive efficiency, instead it can be calculated by comparing the overall kinetic power received on the ToF collector to the corresponding electric power used for acceleration, as shown in

$$\eta_{poly} = \frac{\sum \frac{1}{2}\dot{m}_t v_t^2}{V_{ac} I_t} = \frac{\sum \frac{T_t^2}{2\dot{m}_t}}{V_{ac} I_t} \tag{14}$$

where $\sum \frac{1}{2}\dot{m}_t v_t^2$ is the kinetic power of the particles received on the ToF collector, and I_t is the initial overall current received on the ToF collector. Applying this method to the same example above, the case with a P4 grade emitter at +3000 V, the calculated polydispersive efficiency is 0.917, which is slightly lower than the previous calculation as it also takes into account the fragmentation effects.

Table 4 summarizes the efficiency components discussed in this section. As for other efficiency components, the non-kinetic efficiency consists of voltage losses over the resistance over the liquid propellant on the emitter, and it is typically calculated using a retarding potential analyser to measurement its plume energy distribution; the ionization efficiency need to take the fragmentation effects into consideration, which also requires the measurement of a retarding potential analyser; the angular efficiency needs to be calculated from the angular distribution of plume current density. These other efficiency components will be studied in future work.

VIII. Conclusion

The PET-100-MK1 electrospray thruster was studied in this paper. The thruster was manufactured using low-cost techniques, and featuring a compact design with a passive propellant transport method. The electropray emitters were manufactured using CNC machining. In total four types of emitters were investigated, including single-tip emitters made of P4 grade porous borosilicate material, 25-tip emitters made of P4 grade material and 100-tip emitters made of P4 and P5 materials. The emitters were tested in bipolar mode and demonstrated relatively high emission current density especially at high voltages, up to over ±30 μA per tip at ±3500 V. Compared to the emitters made from P5 grade porous glass material, the P4 grade emitters with blunter tips had higher onset voltages and also had exceptional total emission current.

A time-of-flight system was used to characterize the plume particle properties of the PET-100-MK1 thruster. Tests were done with different thruster configurations and at different operating voltages. The ToF measurements clearly demonstrated that purely ionic emission was achieved with certain thruster configurations and operating conditions, including P4-1-tip emitter at -2700 V, P4-25-tip emitter at +3500 V, P4-100-tip emitter at +2500 V, +3000 V and +3500 V, and P5-100-tip emitter at -2000 V, -2200 V and -2600 V. The propulsive performance for per-unit plume current was calculated in these cases, and the overall thruster performance was estimated in a conservative manner assuming the angular efficiency was 80% in all the cases. The specific impulse of the PET-100-MK1 thruster in ionic emission regime was generally within the range from 3000 s to 6000 s, and the estimated thrust ranged from 1.5 μN for single-tip emitter at -2700 V to 204 μN for P4-100-tip emitter at +3500 V. The thrust per emission tip of approximately 2 μN is relatively high compared to most other electrospray thrusters operating in a highly ionic regime.

However, the quality of some ToF measurements conducted in this study needs to be improved. The inductive current generated on the ToF collector created drastic noises to the signal within 10 to 15 μs. A minor proportion of residual current was found in some ToF measurements, suggesting the possibility of droplets' presence in the plume, agreeing with the evidence of liquid accumulation on the extractor at high voltages. In order to confirm this theory, further ToF tests need to be conducted which can record 100% of current decrease over a longer period of time than the 400 μs usually used in this study.

The PET-100-MK1 electrospray thruster demonstrated the capability of operating in purely ionic mode, but the transition conditions of the emission regime from purely ions to droplets need further study. The compact size, the high specific impulse in purely ionic emission regime, and the increased emission density and estimated thrust up to 234 μN make the PET-100-MK1 electrospray thruster potentially a promising option for nanosatellite missions requiring high total velocity change. The PET-100-MK1 thrusters are in the early stages of development, and further work regarding the angular distribution and energy distribution of plume current will be studied in the future.

Acknowledgments

The work has been supported by the Royal Society Grant with the grant number RG150794, the UK Space Agency NSTP Pathfinder Grant under the grant number of NSTP3-PF2-064, the Engineering and Physical Sciences Research Council under the grant number of EP/M508147/1, and the University of Southampton under the funding codes of F2ZEM4, F27K05, F26QTE and F22NS5. The use of the laser profiling system was kindly provided by Dr Kevin Cross at Taicaan Technologies.

References

[1] Gill, E., Sundaramoorthy, P., Bouwmeester, J., Zandbergen, B., and Reinhard, R., "Formation Flying within a Constellation of Nano-Satellites: The QB50 Mission," Acta Astronautica, Vol. 82, No. 1, 2013, pp. 110–117. https://doi.org/10.1016/j.actaastro.2012.04.029.

[2] Selva, D., and Krejci, D., "A Survey and Assessment of the Capabilities of Cubesats for Earth Observation," Acta Astronautica, Vol. 74, 2012, pp. 50–68. https://doi.org/10.1016/j.actaastro.2011.12.014.

[3] Staehle, R. L., Blaney, D., Hemmati, H., Jones, D., Klesh, A., Liewer, P., Lazio, J., Wen-Yu Lo, M., Mouroulis, P., Murphy, N., Pingree, P. J., Wilson, T., Anderson, B., Channing Chow, C., II, Betts, B., Friedman, L., Puig-Suari, J., Williams, A., and Svitek, T., "Interplanetary CubeSats: Opening the Solar System to a Broad Community at Lower Cost," Journal of Small Satellites, Vol. 2, 2013, pp. 161–186.

[4] Lemmer, K., "Propulsion for CubeSats," Acta Astronautica, Vol. 134, No. January, 2017, pp. 231–243. https://doi.org/10.1016/j.actaastro.2017.01.048.

[5] Krejci, D., and Lozano, P., "Space Propulsion Technology for Small Spacecraft," Proceedings of the IEEE, Vol. 106, No. 3, 2018, pp. 362–378. https://doi.org/10.1109/JPROC.2017.2778747.

[6] Krejci, D., and Lozano, P., "Micro-machined Ionic Liquid Electrospray Thrusters for Cubesat Applications," Proceedings of the 35th International Electric Propulsion Conference, IEPC-2017-224, Electric Rocket Propulsion Society, Atlanta, Georgia, 2017.

[7] Bock, D., and Tajmar, M., "Highly Miniaturized FEEP Propulsion System (NanoFEEP) for Attitude and Orbit Control of Cubesats," Acta Astronautica, Vol. 144, 2018, pp. 422–428. https://doi.org/10.1016/j.actaastro.2018.01.012.

[8] Krejci, D., Mier-Hicks, F., Thomas, R., Haag, T., and Lozano, P., "Emission Characteristics of Passively Fed Electrospray Microthrusters with Propellant Reservoirs," Journal of Spacecraft and Rockets, Vol. 54, 2017, pp. 447–458. https://doi.org/10.2514/1.A33531.

[9] Shagayda, A. A., "On Scaling of Hall Effect Thrusters," IEEE Transactions on Plasma Science, Vol. 43, No. 1, 2015, pp. 12–28. https://doi.org/10.1109/TPS.2014.2315851.

[10] Petro, E. M., and Sedwick, R. J., "Survey of Moderate-Power Electric Propulsion Systems," Journal of Spacecraft and Rockets, Vol. 54, No. 3, 2017, pp. 529–541. https://doi.org/10.2514/1.A33647.

[11] Gomez Jenkins, M., Krejci, D., and Lozano, P., "CubeSat Constellation Management Using Ionic Liquid Electrospray Propulsion," Acta Astronautica, Vol. 151, 2018, pp. 243–252. http://doi.org/10.1016/j.actaastro.2018.06.007.

[12] Hill, F. A., Heubel, E. V., Ponce de Leon, P., and Velasquez-Garcia, L. F., "High-Throughput Ionic Liquid Ion Sources Using Arrays of Microfabricated Electrospray Emitters with Integrated Extractor Grid and Carbon Nanotube Flow Control Structures," Journal of Microelectromechanical Systems, Vol. 23, No. 5, 2014, pp. 1237–1248. http://doi.org/10.1109/JMEMS.2014.2320509.

[13] Romero-Sanz, I., Bocanegra, R., Fernandez de la Mora, J., and Gamero-Castaño, M., "Source of Heavy Molecular Ions Based on Taylor Cones of Ionic Liquids Operating in the Pure Ion Evaporation Regime," Journal of Applied Physics, Vol. 94, No. 5, 2003, pp. 3599–3605. http://doi.org/10.1063/1.1598281.

[14] Castro, S., Larriba, C., De La Mora, J. F., Lozano, P., Sümer, S., Yoshida, Y., and Saito, G., "Effect of Liquid Properties on Electrosprays from Externally Wetted Ionic Liquid Ion Sources," Journal of Applied Physics, Vol. 102, No. 9, 2007. http://doi.org/10.1063/1.2802547.

[15] Krpoun, R., "Micromachined Electrospray Thrusters for Spacecraft Propulsion," Ph.D. Dissertation, Ecole Polytechnique Federale De Lausanne, Switzerland, 2009. https://infoscience.epfl.ch/record/128798.

[16] Krejci, D., Mier-Hicks, F., Thomas, R., Haag, T., and Lozano, P., "Emission Characteristics of Passively Fed Electrospray Microthrusters with Propellant Reservoirs," Journal of Spacecraft and Rockets, Vol. 54, 2017, pp. 447–458. http://doi.org/10.2514/1.A33531.

[17] Lozano, P., and Martínez-Sánchez, M., "Ionic Liquid Ion Sources: Characterization of Externally Wetted Emitters," Journal of Colloid and Interface Science, Vol. 282, No. 2, 2005, pp. 415–421. http://doi.org/10.1016/j.jcis.2004.08.132.

[18] Brikner, N., and Lozano, P. C., "The Role of Upstream Distal Electrodes in Mitigating Electrochemical Degradation of Ionic Liquid Ion Sources," Applied Physics Letters, Vol. 101, No. 19, 2012, pp. 1–4. https://doi.org/10.1063/1.4766293.

[19] Courtney, D. G., and Shea, H., "Influences of Porous Reservoir Laplace Pressure on Emissions from Passively Fed Ionic Liquid Electrospray Sources," Applied Physics Letters, Vol. 107, No. 10, 2015, pp. 1–5. https://doi.org/10.1063/1.4930231.

[20] Lenguito, G., Fernandez de la Mora, J., and Gomez, A., "Scaling up the Power of an Electrospray Microthruster," Journal of Micromechanics and Microengineering, Vol. 24, No. 5, 2014, pp. 1–10. http://doi.org/10.1088/0960-1317/24/5/055003.

[21] Guerra-Garcia, C., Krejci, D., and Lozano, P., "Spatial Uniformity of the Current Emitted by an Array of Passively Fed Electrospray Porous Emitters," Journal of Physics D: Applied Physics, Vol. 49, No. 11, 2016, pp. 1–12. http://doi.org/10.1088/0022-3727/49/11/115503.

[22] Courtney, D. G., Alvarez, N., and Demmons, N. R., "Electrospray Thrusters for Small Spacecraft Control: Pulsed and Steady State Operation," 2018 Joint Propulsion Conference, AIAA 2018-4654, Cincinnati, Ohio, 2018, pp. 1–15. http://doi.org/10.2514/6.2018-4654.

[23] Legge, R. S., and Lozano, P. C., "Electrospray Propulsion Based on Emitters Microfabricated in Porous Metals," Journal of Propulsion and Power, Vol. 27, No. 2, 2011, pp. 485–495. http://doi.org/10.2514/1.50037.

[24] Courtney, D. G., Li, H. Q., and Lozano, P., "Emission Measurements from Planar Arrays of Porous Ionic Liquid Ion Sources," Journal of Physics D: Applied Physics, Vol. 45, No. 48, 2012, pp. 1–13. https://doi.org/10.1088/0022-3727/45/48/485203.

[25] Dandavino, S., Ataman, C., Ryan, C., Chakraborty, S., Courtney, D. G., Stark, J. P. W., and Shea, H. R., "Microfabricated Electrospray Emitter Arrays with Integrated Extractor and Accelerator Electrodes for the Propulsion of Small Spacecraft," Journal of Micromechanics and Microengineering, Vol. 24, No. 7, 2014, pp. 1–13. https://doi.org/10.1088/0960-1317/24/7/075011.

[26] Legge Jr, R., "Fabrication and Characterization of Porous Metal Emitters for Electrospray Applications," Ph.D. Dissertation, Massachusetts Institute of Technology, 2008. http://hdl.handle.net/1721.1/45301.

[27] Courtney, D. G., Dandavino, S., and Shea, H. R., "Comparing Direct and Indirect Thrust Measurements from Passively Fed and Highly Ionic Electrospray Thrusters," Journal of Propulsion and Power, Vol. 32, No. 2, 2016, pp. 392–407. https://doi.org/10.2514/1.B35836.

[28] Xie, J., Canonica, M. D., and Lozano, P. C., "Fabrication of Electrospray Thrusters by Sintering Glass Microspheres," 49th AIAA/ASME/SAE/ASEE Joint Propulsion Conference and Exhibit, AIAA 2013-3824, San Jose, CA, 2013, pp. 1–8. https://doi.org/10.2514/6.2013-3824.

[29] Lozano, P. C., "Energy Properties of an EMI-Im Ionic Liquid Ion Source," Journal of Physics D: Applied Physics, Vol. 39, No. 1, 2005, pp. 126–134.
https://doi.org/10.1088/0022-3727/39/1/020.

[30] Natisin, M. R., and Zamora, H. L., "Performance of a Fully Conventionally Machined Liquid-Ion Electrospray Thruster Operated in PIR," Proceedings of the 36th International Electric Propulsion Conference 2019, IEPC-2019-522, Electric Rocket Propulsion Society, Vienna, Austria, 2019, pp. 1–16.

[31] Courtney, D. G., and Shea, H., "Fragmentation in Time-of-Flight Spectrometry-Based Calculations of Ionic Electrospray Thruster Performance," Journal of Propulsion and Power, Vol. 31, No. 5, 2015, pp. 1500–1504.
https://doi.org/10.2514/1.B35837.

[32] Lozano, P., and Martinez-Sanchez, M., "Efficiency Estimation of EMI-BF4 Ionic Liquid Electrospray Thrusters," Proceedings of the 41st AIAA/ASME/SAE/ASEE Joint Propulsion Conference & Exhibit, AIAA 2005-4388, Tucson, Arlzona, 2005.
https://doi.org/10.2514/6.2005-4388.

[33] Lozano, P., "Studies on the Ion-Droplet Mixed Regime in Colloid Thrusters," Ph.D. Dissertation, Massachusetts Institute of Technology, 2003.
http://hdl.handle.net/1721.1/16994.